

Article

Thermal Stability of Polycaprolactone Grafted Densely with Maleic Anhydride Analysed Using the Coats–Redfern Equation

Kotchaporn Thangunpai ¹, Donghao Hu ^{2,3,*}, Xianlong Su ³, Mikio Kajiyama ², Marcos A. Neves ²
and Toshiharu Enomae ^{2,*}

¹ Graduate School of Science and Technology, University of Tsukuba, 1-1-1 Tennodai, Tsukuba 305-8572, Ibaraki, Japan

² Faculty of Life and Environmental Science, University of Tsukuba, 1-1-1 Tennodai, Tsukuba 305-8572, Ibaraki, Japan

³ Department of Chemistry & State Key Laboratory of Molecular Engineering of Polymers, Fudan University, Shanghai 200433, China

* Correspondence: hudonghao@fudan.edu.cn (D.H.); enomae.toshiharu.fw@u.tsukuba.ac.jp (T.E.)

Abstract: The plastic waste problem has recently attracted unprecedented attention globally. To reduce the adverse effects on environments, biodegradable polymers have been studied to solve the problems. Poly(ϵ -caprolactone) (PCL) is one of the common biodegradable plastics used on its own or blended with natural polymers because of its excellent properties after blending. However, PCL and natural polymers are difficult to blend due to the polymers' properties. Grafted polymerization of maleic anhydride and dibenzoyl peroxide (DBPO) with PCL is one of the improvements used for blending immiscible polymers. In this study, we first focused on the effects of three factors (stirring time, maleic anhydride (MA) amount and benzoyl peroxide amount) on the grafting ratio with a maximum value of 4.16% when applying 3.000 g MA and 1.120 g DBPO to 3.375 g PCL with a stirring time of 18 h. After that, the grafting condition was studied based on the kinetic thermal decomposition and activation energy by the Coats–Redfern method. The optimal fitting model was confirmed by the determination coefficient of nearly 1 to explain the contracting volume mechanism of synthesized PCL-g-MA. Consequently, grafted MA hydrophilically augmented PCL as the reduced contact angle of water suggests, facilitating the creation of a plastic–biomaterial composite.

Keywords: Coats–Redfern equation; grafting; maleic anhydride; poly(ϵ -caprolactone); thermal stability



Citation: Thangunpai, K.; Hu, D.; Su, X.; Kajiyama, M.; Neves, M.A.; Enomae, T. Thermal Stability of Polycaprolactone Grafted Densely with Maleic Anhydride Analysed Using the Coats–Redfern Equation. *Polymers* **2022**, *14*, 4100. <https://doi.org/10.3390/polym14194100>

Academic Editors: Mariola Robakowska, Łukasz Gierz and Anna Modrzejewska-Sikorska

Received: 31 August 2022

Accepted: 26 September 2022

Published: 30 September 2022

Publisher's Note: MDPI stays neutral with regard to jurisdictional claims in published maps and institutional affiliations.



Copyright: © 2022 by the authors. Licensee MDPI, Basel, Switzerland. This article is an open access article distributed under the terms and conditions of the Creative Commons Attribution (CC BY) license (<https://creativecommons.org/licenses/by/4.0/>).

1. Introduction

Benefiting from their outstanding physical and chemical properties, such as flexibility, light weight and low cost, plastics have played an extremely important role in modern society [1–5]. However, with more and more common nondegradable types of plastics (such as polyethylene (PE), polypropylene (PP), polystyrene (PS) and polyvinyl chloride (PVC)) being produced, unrecycled plastic waste has become a crucial problem all over the world [6–10], causing many environmental and health problems [11–16]. According to the reports from the Organization for Economic Co-operation and Development (OECD), 6300 mega tons of plastics was produced between 1950 and 2015, while more than 80% of those were accumulated in landfills or left in the natural environment [17]. These problems were affected by the recalcitrant nature that makes the plastic waste unyielding to biodegradation due to its longer duration of degradation time [18]. Since the early 1970s, many studies and regulations related to plastic waste issues have been carried out to solve this problem [19–21]. One of these to focus on and to try to develop is biodegradable polymers. Biodegradable polymers can be classified into two main groups: natural polymers (e.g., polysaccharides, proteins and nucleic acids) and synthetic polymers (e.g., polyester: polycaprolactone and poly (amino acids)) [22–24].

Poly(ϵ -caprolactone) (PCL) is a biodegradable semi-crystalline synthetic polyester with excellent biocompatibility, flexibility and thermo-plasticity properties [25]. Various applications of it and relevant copolymers have been reported, such as drug delivery systems [26–30] and adhesives for bookbinding and packaging [31–33]. PCL can be degraded within several months to several years depending on the molecular weight, natural environment conditions, pH, purity, thickness and so on [34–36]. Attempts have also been made to blend PCL widely with natural polymers such as polysaccharides that constitute paper materials and proteins to improve the properties of biodegradable polymers. However, the two different kinds of polymers are rather immiscible due to their lack of affinity [37]. To improve the blending affinity of immiscible polymers, graft polymerization is commonly applied as an effective method of modifying the physicochemical interactions and phase dispersion between the blending components. Graft polymerization can be induced by the attaching of monomers to the surface of polymers through covalent bonds [38] with suitable unsaturated polar functional groups, such as amines, and anhydrides [39,40].

A maleated component is a functional site usually consisting of some polar groups to increase interfacial adhesion and/or interaction between two or more components [41]. Representatives are maleic anhydride (MA), glycidyl methacrylate, acrylic acid and oxazoline. The most preferred is MA from the aspect of the facilitated modification of polymers since it is easy-to-handle, low toxic, not likely to be homopolymerized during a mild free radical melt-grafting and highly miscible when the components are combined [41,42]. The reaction of MA groups can be produced in the presence of a peroxide radical initiator through a grafting reaction in any of the melt phases, solid state, suspension/emulsion and solution. Among them, the solution grafting proceeds in a solvent for suitably dissolving a reactant polymer and provides high grafting ratios without degradation of the polymer during the reaction [43,44]. In addition, a peroxide radical initiator is required to exert a crucial effect on the grafting polymer process. In the grafting processes, the initial reaction induced by the initiator is the dehydrogenation of hydrogen atoms from α -carbon atoms to the ester carbonyl groups to form polymeric macroradicals. Then, the end of the radical chain also forms the macromer molecules via β -scissoring [45]. Dibenzoyl peroxide (DBPO) is one of the initiators widely used for grafting reactions because of its slow initiator decomposition rate at a suitable reaction temperature [41].

The thermal stability of a biodegradable polymer is one of the essential factors reflecting their degradation feasibility [46]. The thermal response and combustion characteristics obtained from important reaction kinetic parameters, such as activation energy, reaction order and pre-exponential factor, can be applied to exhibit the thermal stability and give guidance for the synthesis of biodegradable polymers [47]. To determine, calculate and explain the decomposition mechanisms from the aspect of the study of solid-state kinetics, the reaction models of the monomer, polymer or copolymer before and after blending have been studied. Kinetic studies have been conducted using thermal analysis (TGA/DTA) to estimate the thermal stability of the polymer. The Coats–Redfern (CR) kinetic model is a common integral method and has been applied to the studies of the thermal decomposition of coal and biomass [48–50]. The TGA/DTA data (weight loss, heating rate, etc.) was used to evaluate the kinetic parameters of solid-state reactions. The accurate and precision temperature measurement was conducted and calculated from a linear heating rate because of endo- or exo-thermic reactions [51].

In this research, we focused on an optimum condition for the synthesis of PCL grafted with MA (PCL-g-MA) with the highest possible grafting ratio. Consequently, the highest grafting ratio helps explain the thermal decomposition model and activation energy using the CR model. In addition, the highest grafting ratio is expected to provide the highest hydrophilicity to the plastic so that the surface is hydrophilically augmented to be more miscible with hydrophilic materials such as paper and other biomass.

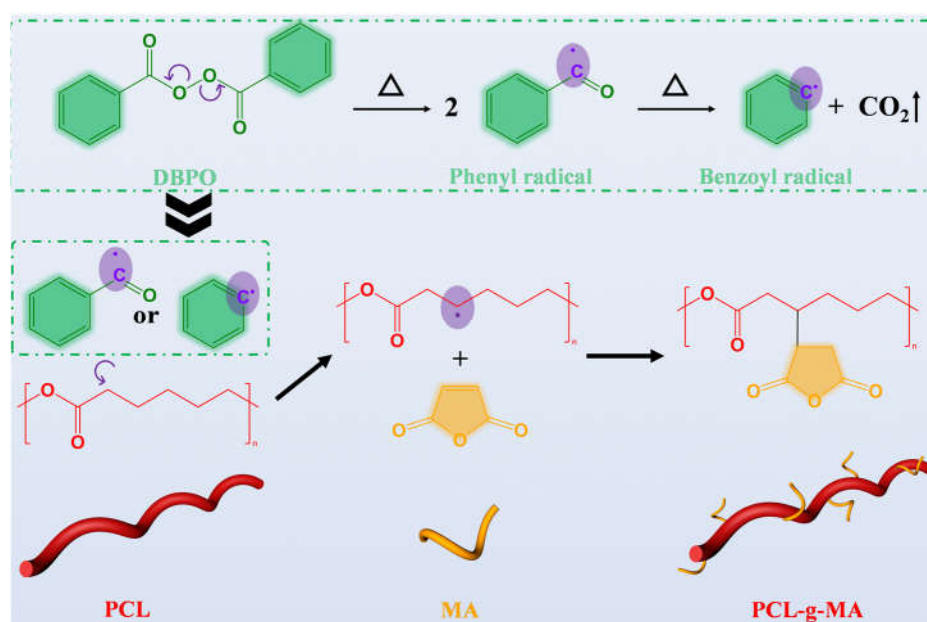
2. Materials and Methods

2.1. Materials

PCL ($M_w = 10,000$ g/mol), DBPO, MA ($M_w = 98.06$ g/mol), tetrahydrofuran (THF), hexane, potassium hydroxide (KOH), ethanol (C_2H_5OH) and phenolphthalein ethanol solution (1.0% *w/v*) were purchased from Fujifilm Wako Pure Chemical (Osaka, Japan). A filter paper (No.4, Monotaro, Kiriya, Japan) was utilized for the experiment.

2.2. Synthesis of PCL-g-MA

The synthesis of MA-grafted PCL (PCL-g-MA) was modified based on a previous study [52]. Benzoyloxy radicals were produced by the homolysis of DBPO. Then, DBPO-free radicals attack the PCL molecule to generate PCL radicals. Finally, MA moieties react to the PCL radicals (Scheme 1).



Scheme 1. Grafting reaction of MA onto PCL.

In the experiment, 3.375 g PCL and a mass of MA specified in following tables were weighed precisely and dissolved in 40 mL THF at 40 ± 2 °C for 30 min in an oil bath under an N_2 atmosphere. DBPO was then added and stirred for various periods. The condition was grouped into three factors in Tables 1–3.

Table 1. Experimental design for the factor of stirring time.

Sample	Time (h)	Amount of DBPO (g)	Amount of MA (g)
t1	3	1.120	3.000
t2	6	1.120	3.000
t3	9	1.120	3.000
t4	12	1.120	3.000
t5	15	1.120	3.000
t6	18	1.120	3.000
t7	21	1.120	3.000
t8	24	1.120	3.000

Table 2. Experimental design for the factor of the addition amount of MA.

Sample	Time (h)	Amount of DBPO (g)	Amount of MA (g)
M1	18	1.120	0.165
M2	18	1.120	0.331
M3	18	1.120	0.827
M4	18	1.120	1.655
M5 (t6)	18	1.120	3.000
M6	18	1.120	4.500
M7	18	1.120	6.754

Table 3. Experimental design for the factor of the addition amount of DBPO.

Sample	Time (h)	Amount of DBPO (g)	Amount of MA (g)
B1	18	0.297	3.000
B2	18	0.709	3.000
B3 (t6)	18	1.120	3.000
B4	18	1.784	3.000
B5	18	2.738	3.000

After that, the THF solution of PCL, DBPO and MA was poured into hexane (1:10 *v/v*) and was gently stirred to precipitate the compounds at 25 °C for 10 min. Finally, the precipitated polymer was filtrated and dried in a vacuum desiccator at 25 °C. For each of the series, an optimum condition was screened.

2.3. Characterization

2.3.1. Fourier Transform Infrared Spectroscopy (FTIR)

The functional groups of the samples were identified with an FTIR spectrophotometer (FT/IR-6100, JEOL, Tokyo, Japan) in the range of 500–4000 cm^{-1} . Subsequently, pellets of the PCL-g-MA specimens mixed with KBr (1:100 *w/w*) were prepared, dried in a desiccator for 24 h and subjected to the FTIR measurement.

2.3.2. X-Ray Photoelectron Spectroscopy (XPS)

The surface compositions of the specimens were further analysed by X-ray photoelectron spectroscopy (XPS) (JPS-9010TR, JEOL, Tokyo, Japan) with an $\text{AlK}\alpha$ radiation (1486.6 eV) source at 10 kV and 20 mA.

2.3.3. Determination of Grafting Ratio

A total of 2 g of the synthesized polymer was heated in 200 mL THF at 40 ± 2 °C for 2 h. Subsequently, the heated solution was immediately titrated with a 0.03 M ethanolic KOH solution with phenolphthalein as an indicator. The MA loading percentage in the solution was applied to calculate the acid number and grafting ratio by Equations (1) and (2) [53]:

$$\text{Acid number (mgKOH/g)} = \frac{C_{\text{KOH}}(\text{M}) \times V_{\text{KOH}}(\text{mL}) \times 56.1}{m(\text{polymer}(\text{g}))}, \quad (1)$$

where C_{KOH} is the concentration of ethanolic KOH solution ($\text{mol}\cdot\text{L}^{-1}$), V_{KOH} is the PCL-g-MA titrate volume (mL), m (polymer) is the mass of copolymer (g).

$$\text{Grafting ratio (\%)} = \frac{\text{Acid number} \times 98.1}{2 \times 561}. \quad (2)$$

2.3.4. Field Emission Scanning Electron Microscope (FESEM)

Samples were coated with platinum (Pt) using a sputter before the observation with a field emission scanning electron microscope (SU8020, Hitachi, Tokyo, Japan).

2.3.5. Contact Angle Measurement

Contact angle (CA) measurement was carried out with PCL and PCL-g-MA coated on a glass surface by a sessile drop method (DropMaster DMS-401, Kyowa Interface Science, Saitama, Japan). Deionized water with a volume of approx. 20 μL was dropped on the surface of them. The measurement was conducted at the interface between air and deionized water.

2.3.6. Thermal Property Measurement (TGA/DTG/DSC)

Thermogravimetric analysis (TGA) was conducted with a thermogravimetric analyser (TG/DTA7300, Seiko Instruments Inc., Chiba, Japan) and heated up to 550 $^{\circ}\text{C}$ at a heating rate of 15 $^{\circ}\text{C}/\text{min}$ and a flow rate of 200 mL/min of argon gas. The differential scanning calorimetry (DSC) (X-DSC-7000, Shimadzu, Kyoto, Japan) curves were determined during heating (10–110 $^{\circ}\text{C}$) and cooling (110 to -20 $^{\circ}\text{C}$) processes under the same atmosphere. The crystallinities (X_c) of PCL and each synthesized PCL-g-MA were calculated using the standard enthalpy of PCL ($\Delta H_m = 139.5$ J/g) [54]. X_c was calculated based on the ratio of the enthalpy of synthesized PCL-g-MA to that of pure PCL.

2.3.7. The Coats–Redfern Equation [51]

The effect of an absorbed dose on the thermal stability of PCL-g-MA was evaluated from the aspect of the thermal properties obtained by TGA and DTA. The absorbed doses were varied by changing the heating rate of TGA and DTA from 5–30 $^{\circ}\text{C}/\text{min}$ in each condition.

Theoretical analysis

The rate of a solid-state reaction can be represented by the Arrhenius plot expressed from Equation (3):

$$\frac{d\alpha}{dt} = A e^{-\frac{E_a}{RT}} f(\alpha), \quad (3)$$

where A is the pre-exponential factor, E_a is the activation energy, T is the absolute temperature, R is the gas constant, $f(\alpha)$ is the differential conversion function and α is the conversion fraction from the gravimetric measurement, which is defined as Equation (4) [55]:

$$\alpha = \frac{m_0 - m_t}{m_0 - m_f}, \quad (4)$$

where m_0 , m_t and m_f are the initial weight, the weight at a given time t and the final weight, respectively.

In general, the kinetic analysis is conducted using the iso-conversional method, which assumes that the reaction rate is a function of only temperature as the independent variable and can be classified into two sub-methods.

Isothermal method

Equation (5) is obtained by integrating the rate under isothermal conditions:

$$\ln(t) = \ln\left[\frac{g(\alpha)}{A}\right] + \frac{E_a}{RT}, \quad (5)$$

where $g(\alpha)$ is the integral conversion function defined as Equation (6):

$$g(\alpha) = \int_0^{\alpha} \frac{d\alpha}{f(\alpha)}, \quad (6)$$

From Equation (5), E_a and the constant $\ln[g(\alpha)/A]$ can be obtained from the slope and the intercept of the linear relationship between $\ln(t)$ and T^{-1} for $\alpha = \text{constant}$.

Nonisothermal method

The reaction rate can be represented in the nonisothermal condition as Equation (7):

$$g(\alpha) = \frac{A}{\beta} \int_0^T e^{-\left(\frac{E_a}{RT}\right)} dT, \quad (7)$$

where β is the heating rate.

By using the Coats–Redfern equation to solve Equation (7) when $2RT/E \ll 1$, the reordered equation can be rewritten as Equation (8):

$$\ln \frac{g(\alpha)}{T^2} = \ln \left(\frac{AR}{\beta E} \right) - \frac{E_a}{RT}. \quad (8)$$

The TGA data of the maximum grafting ratio of PCL-g-MA were calculated by using the Coats–Redfern Equation to study the synthesis process model. The linear regression is represented by $\ln[g(\alpha)/T^2]$ as a function of T^{-1} to determine E_a and A from the slope and the intercept, respectively. The algebraic expressions of $f(\alpha)$ and $g(\alpha)$ for the kinetic models are listed in Table 4 [56–59].

Table 4. Thermal kinetic models for solid-state kinetics with expression for $f(\alpha)$ and $g(\alpha)$.

Mechanism Model	Differential Form $f(\alpha)$	Integral Form $g(\alpha)$
Order of Reaction		
First order (F1)	$1 - \alpha$	$-\ln(1 - \alpha)$
Second order (F2)	$(1 - \alpha)^2$	$(1 - \alpha)^{-1} - 1$
Third order (F3)	$(1 - \alpha)^3$	$[(1 - \alpha)^{-2} - 1]/2$
Diffusion Models		
One-dimensional diffusion (D1)	$1/2\alpha$	α^2
Two-dimensional diffusion (D2)	$[-\ln(1 - \alpha)]^{-1}$	$[(1 - \alpha)\ln(1 - \alpha)] + \alpha$
Three-dimensional diffusion, Jandel (D3)	$3(1 - \alpha)^{2/3}/[2(1 - (1 - \alpha)^{1/3})]$	$[1 - (1 - \alpha)^{1/3}]^2$
Diffusion control, Ginstling–Brounshtein (D4)	$3/2[(1 - \alpha)^{-1/3} - 1]$	$1 - (2\alpha/3) - (1 - \alpha)^{2/3}$
Nucleation Growth Models		
Two-dimensional (A2)	$2(1 - \alpha)[-\ln(1 - \alpha)]^{1/2}$	$[-\ln(1 - \alpha)]^{1/2}$
Three-dimensional (A3)	$3(1 - \alpha)[-\ln(1 - \alpha)]^{3/2}$	$[-\ln(1 - \alpha)]^{1/3}$
Four-dimensional (A4)	$4(1 - \alpha)[-\ln(1 - \alpha)]^{3/4}$	$[-\ln(1 - \alpha)]^{1/4}$
Geometrical Contraction Model		
One dimension (R1)	1	A
Two dimensions (R2)	$2(1 - \alpha)^{1/2}$	$1 - (1 - \alpha)^{1/2}$
Three dimensions (R3)	$2(1 - \alpha)^{1/2}$	$1 - (1 - \alpha)^{1/3}$
Experimental Nucleation Models		
Power law (P2)	$2\alpha^{1/2}$	$\alpha^{1/2}$
Power law (P3)	$3\alpha^{2/3}$	$\alpha^{1/3}$
Power law (P4)	$4\alpha^{3/4}$	$\alpha^{1/4}$

3. Results and Discussion

3.1. Infrared Spectroscopy (FTIR)

Figure 1 shows the FTIR spectra of PCL, MA and PCL-g-MA synthesized with the mentioned different experimental conditions. PCL showed the characteristic peak of hydroxyl groups at 3444 cm^{-1} . Two distinct peaks at 2952 and 2869 cm^{-1} corresponded to

the asymmetrical and symmetrical stretching of CH_2 , respectively. As for MA, the $\text{C}=\text{O}$ peaks of MA were found at 1861 (low intensity) and 1785 cm^{-1} (medium intensity) due to the $\text{C}=\text{O}$ stretching group of low and high intensity hydrolysed MA, respectively [60]. PCL-g-MA was successfully generated by grafting MA onto PCL since two characteristic shoulders of anhydride carboxyl groups appeared at 1790 and 1867 cm^{-1} [61]. Additionally, the $\text{C}-\text{O}$ and $\text{C}-\text{C}$ stretchings were located at 1298 and 1244 cm^{-1} , respectively, while the combination asymmetric $\text{C}-\text{O}-\text{C}$ stretching and the symmetric $\text{C}-\text{O}-\text{C}$ stretching peak was located at 1179 cm^{-1} [61,62]. In all spectra, the $\text{C}=\text{O}$ group peaks were present at 1730 cm^{-1} . The above results confirmed a similar tendency to the previous reports [63,64] that MA was successfully grafted onto PCL.

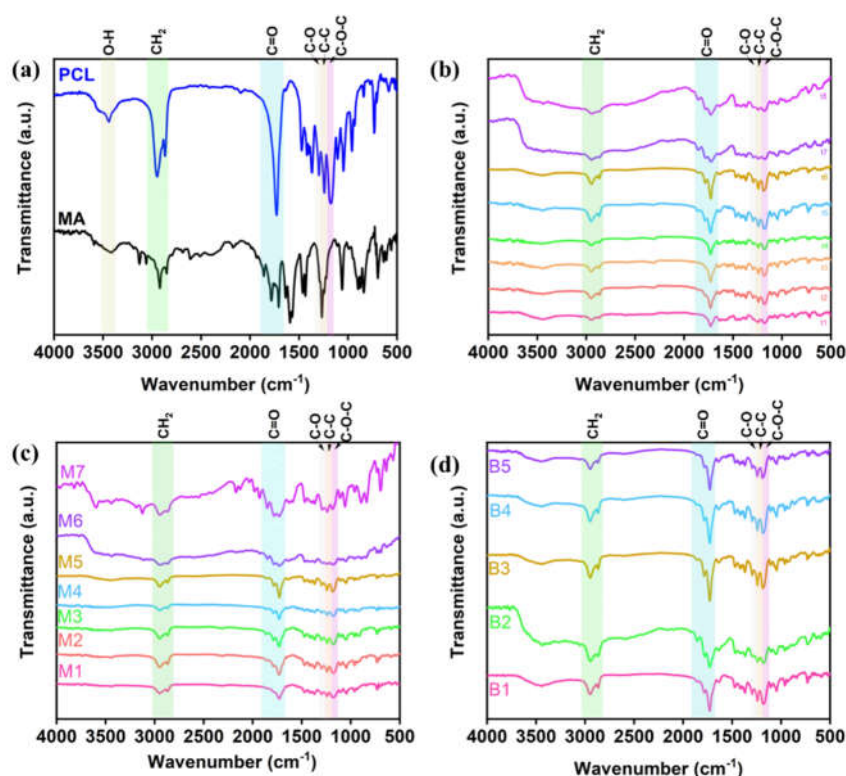


Figure 1. FTIR spectra of (a) PCL and MA, and PCL-g-MA synthesized with different (b) reaction periods, (c) amounts of MA and (d) amounts of DBPO.

3.2. XPS

The surface physicochemical properties were further confirmed by XPS analysis. Figure 2a shows the XPS full spectra of PCL, MA and PCL-g-MA with two corresponding peaks, C_{1s} (approx. 287 eV) and O_{1s} (approx. 534 eV), along with their relative atomic composition ratios. Figure 2b–g shows the C_{1s} and O_{1s} spectra of PCL, MA and PCL-g-MA. The C_{1s} spectrum of PCL in Figure 2b indicates three groups, including $-\text{CH}_x$ (284.5 eV), $-\text{C}-\text{O}-$ (286.3 eV) and $-\text{C}(=\text{O})-\text{O}-$ (288.5 eV) [65]. The O_{1s} peaks (Figure 2c) are identified at 533.7 and 535.0 eV, corresponding to $-\text{C}=\text{O}$ and $-\text{C}-\text{O}-$, respectively. The C_{1s} spectrum of MA (Figure 2d) is in accordance with the same three kinds of groups, $-\text{CH}_x$ (286.7 eV), $-\text{C}-\text{O}-$ (288.2 eV) and $-\text{C}(=\text{O})-\text{O}-$ (290.6 eV). The three peaks consisting of the O_{1s} peak of MA (Figure 2e) appear at 533.8, 535.2 and 534.5 eV, representing the ether oxygen and carbonyl oxygen both in maleic anhydride and the carbonyl bond in the amide unit [66,67], respectively. The C_{1s} and O_{1s} peaks of PCL-g-MA are located at and corresponded to the same kinds of groups as those of PCL and MA (Figure 2f,g). Moreover, the O_{1s} peaks of PCL-g-MA are carbonyl groups of amide units of MA. This also proves that MA was successfully grafted on the surface of PCL. More detailed information is supplied in the supplementary material (Figures S6–S8).

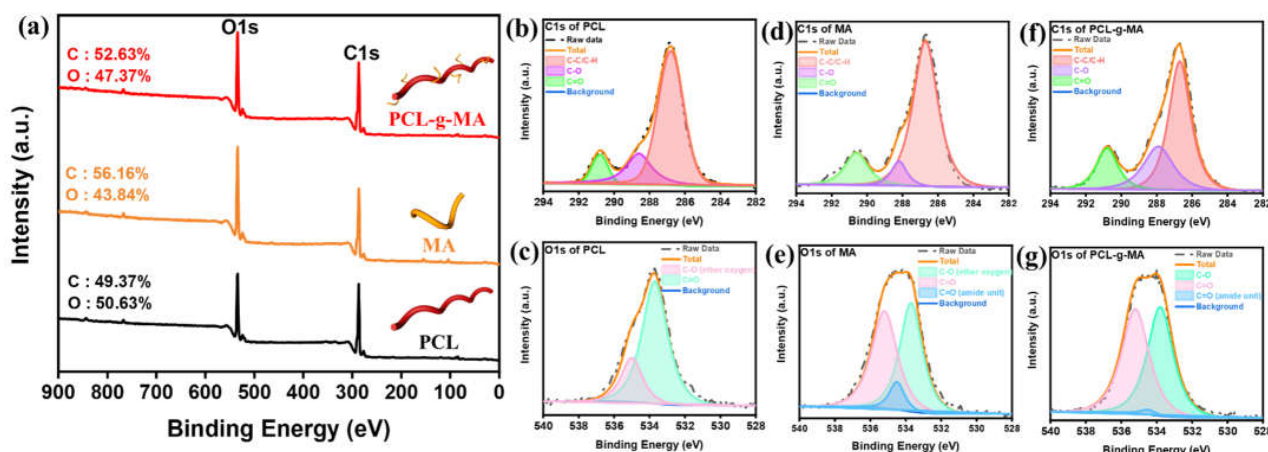


Figure 2. (a) XPS full spectra of PCL, MA and PCL-g-MA, and high-resolution XPS spectra of (b) C_{1s} of PCL, (c) O_{1s} of PCL, (d) C_{1s} of MA, (e) O_{1s} of MA, (f) C_{1s} of PCL-g-MA and (g) O_{1s} of PCL-g-MA prepared by 3.375 g PCL, 3.000 g MA and 1.120 g DBPO by 18 h.

3.3. Determination of Grafting Ratio

Figure 3a shows the grafting ratios of PCL-g-MA with different reaction periods. From the results, the grafting ratio obviously increased from 3 to 18 h, and attained an equilibrium state after 18 h. Figure 3b shows that the grafting ratio increased with the increase in MA amount from 0.165 to 3.000 g, while the reaction period (18 h) and initiator DBPO amount (1.120 g) were kept constant. With the increase in the added MA amount, the chance of PCL reacting with MA became higher [41,68]. In addition, with excess MA (>3.000 g) adopted for the synthesis, the grafting ratio decreased with the increasing MA. This is because overloaded MA could cause the free radicals to undergo a termination or combination reaction with PCL macroradicals, along with some unexpected reactions (such as cage effect), all of which could lead to the reduction in the grafting ratio [69]. Figure 3c shows that the grafting ratio of PCL-g-MA first increased and then decreased with the increasing amount of DBPO (0.0297–1.120 g), which mainly resulted from the increased formation of the higher amount of DBPO that would also help raise the probability of MA transfer to the PCL backbone, resulting in a higher grafting ratio result. However, with the continuous addition of DBPO (>1.120 g), the grafting ratio drastically decreased. On the one hand, an excess of radical initiators has free radical species that can promote a termination or a combination reaction between polymer macroradicals. On the other hand, the excess radical initiators may cause the recombination of polymer radicals due to the formation of the crosslinking structure by carbon–carbon crosslinks and the depolymerization reflected by the acute reduction in molecular weight [70]. Above all, the optimum amount of DBPO, amount of MA and the reaction time for PCL-g-MA synthesis were determined to be 1.120 g, 3.000 g and 18 h, respectively.

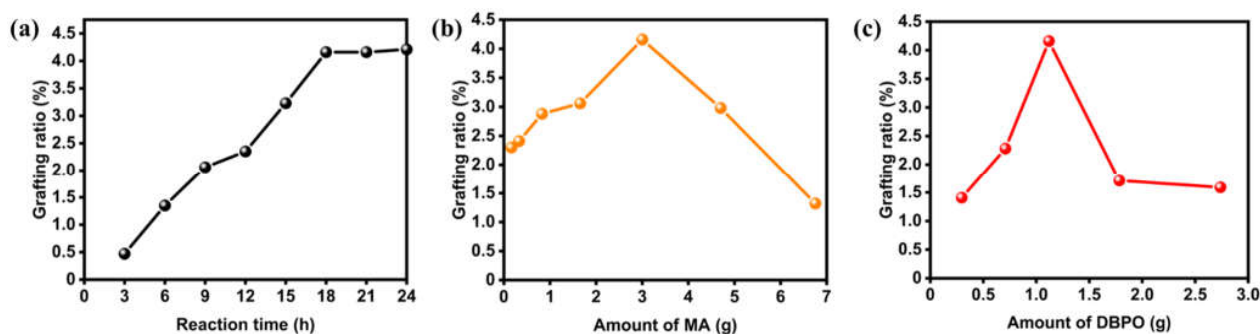


Figure 3. Grafting ratios of PCL-g-MA synthesized with different (a) reaction periods, (b) amounts of MA and (c) amounts of DBPO.

3.4. Morphological Observation

Figure 4a,c show FESEM images featuring the morphology before and after grafting, where a crystallinity (X_c) decrease could be clearly observed. It can be seen from Figure 4a that PCL has mainly fibrous and needle-like crystal structures compared to Figure 4c, PCL-g-MA, that seems to be irregular in shape and has a denser appearance on the surface. The denseness of the surface might result from the bonding between MA and PCL [71]. Meanwhile, the CA results of PCL (Figure 4b) and the synthesised PCL-g-MA (Figure 4d) were 49.9° and 40.4° , respectively. Compared to pure PCL, the surface hydrophilicity and wettability of the PCL-g-MA was enhanced prominently. This property would be expected to facilitate the mixture of PCL-g-MA and cellulosic fibers constituting paper and the creation of biodegradable plastic and paper composites.

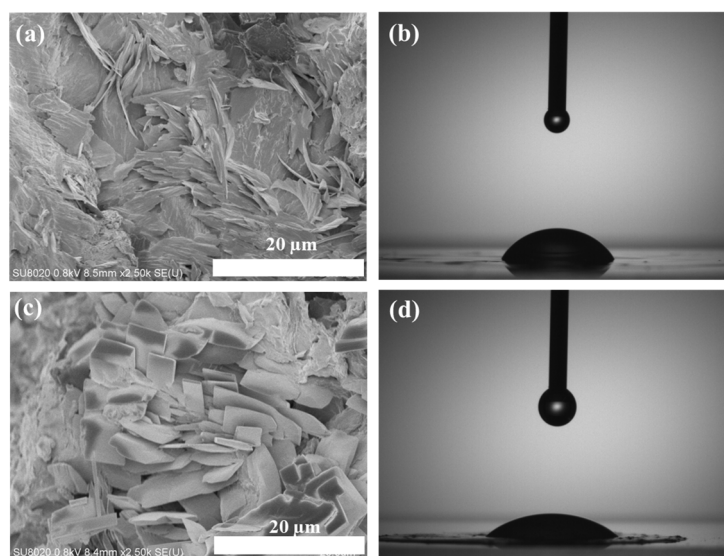


Figure 4. FESEM images of (a) PCL and (b) CA of water on PCL as well as FESEM images in (c) and (d) that on PCL-g-MA synthesized from 3.375 g PCL, 3.000 g MA and 1.120 g DBPO for 18 h.

3.5. DSC

The three parameters derived from the DSC data, the melting temperature (T_m), the enthalpy of melting (ΔH_m) and the X_c were studied to understand the influence of the reaction period, MA amount and DBPO amount on the thermal property of PCL-g-MA. Figure 5 summarizes these parameters when utilizing the reaction period, MA amount and DBPO amount of no more than their individual optimal values. T_m , ΔH_m and X_c decreased with increasing grafting ratio and increasing time. Among them, X_c tended to increase, proving the results obtained from the FESEM images. The grafting ratio refers to the monomers that could be bonded with the covalent bond onto the polymer [72]. Thus, X_c of PCL-g-MA is presumed to be influenced by the addition of MA, which should reduce the degree of crystallinity because MA interacted with plain PCL and inhibited the crystal growth [73]. Figure 5b suggests that T_m , ΔH_m and X_c decreased with an increasing MA amount of addition so that more MA were grafted on principal PCL chains [2]. Figure 5c shows that T_m , ΔH_m and X_c decreased with the increasing amount of DBPO. The increased amount of DBPO increased the MA grafting probability, and then decreased ΔH_m , T_m and X_c of the synthesised PCL-g-MA as compared with those of pure PCL [74]. The reaction time, MA amount and DBPO amount had an influence on the grafting ratio, T_m , ΔH_m and X_c . It is presumed that the higher the latter three parameter values, the lower the grafting ratio.

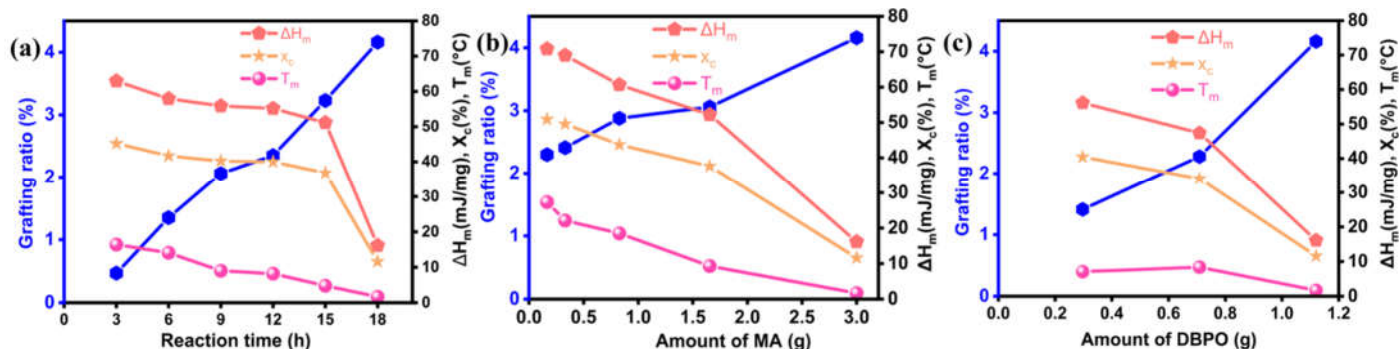


Figure 5. Influence of (a) reaction time, (b) amounts of MA and (c) amounts of DBPO on grafting ratio, T_m , ΔH_m and X_c of synthesized PCL-g-MA.

3.6. Theoretical Analysis Using the Coats–Redfern Method

Figure 6a,b show the TG and DTG curves of pure PCL and MA. Plain PCL shows a large peak in the temperature range of 280–430 $^{\circ}$ C with a maximum degradation temperature (T_{max}) at 378 $^{\circ}$ C due to heat degradation [75]. Pure MA exhibited a mass reduction in the temperature range 62–175 $^{\circ}$ C with a T_{max} at 149 $^{\circ}$ C related to its vaporization [76]. The pure PCL shows two steps of TGA and DTG in Figure 6a,b; the first mass loss (approximately 10%) curve with an onset degradation temperature around 290 $^{\circ}$ C was observed due to the range of PCL at a low molecular weight (short chains) [77]. The major and sharp weight loss of pure PCL occurring in the temperature range of 320–437 $^{\circ}$ C is attributed to a large-scale thermal degradation of the PCL chains [78]. As for PCL-g-MA (Figure 6c,d) at a heating rate of 15 $^{\circ}$ C/min it exhibits two weight loss steps corresponding to MA degradation (106–188 $^{\circ}$ C) and PCL degradation (282–430 $^{\circ}$ C).

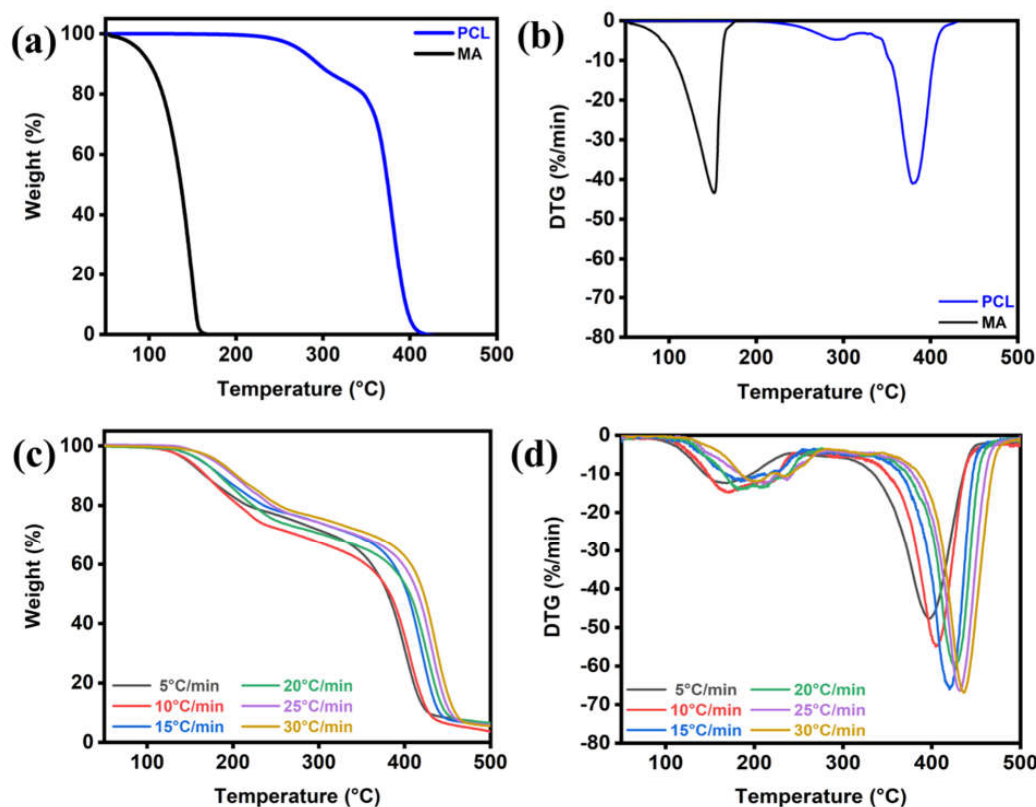


Figure 6. (a) Thermograms and (b) DTG curves of PCL and MA, and (c) thermograms and (d) DTG curves of PCL-g-MA at a maximum grafting ratio all at various heating rates.

In addition, to understand the applicability of the C-R model, TG curves and char residual at 550 °C of a decomposition process for the optimum synthesised PCL-g-MA at different heating rates of 5, 10, 15, 20, 25 and 30 °C/min are compared in Figure 6c, and the DTG curves for the optimum condition to synthesise PCL-g-MA at heating rates of 5, 10, 15, 20, 25 and 30 °C/min are compared in Figure 6d. From the results of TGA and DTG in Figure 6c,d, the thermal decomposition of PCL-g-MA can be divided into two main stages. The first stage indicates MA vaporization at a lower temperature than PCL. Then, the second stage corresponds to the thermal degradation of PCL. All the results of the thermogram characterization of PCL-g-MA initial temperature (T_i), T_{max} , final temperature (T_f) and residue at 550 °C of a decomposition process obtained at different heating rates are summarized in Table S9 (supplementary material part). The above results indicate that with an increasing heating rate, both T_i and T_{max} increased [79]. While there was a small amount of residual ash for PCL-g-MA above 500 °C, there was no residual found in pure PCL and MA. This means that the grafted MA improves the thermal stability of PCL [80]. Thus, T_{max} exists in the range from 396 to 435 °C and seems to reflect the PCL structure. All PCL-g-MA samples underwent less weight loss than PCL because the MA portion tends not to degrade. The further information corresponding to the TGA curves of PCL and PCL-g-MA (Figure 6a,c) is summarized in Table S9 (supplementary material part). It is observed that T_{max} of pure PCL was only 378 °C, while PCL-g-MA showed a higher T_{max} of 420 °C. The higher T_{max} obtained with PCL-g-MA indicates that the MA grafted on the PCL chain improves the thermal stability of the copolymer [80]. The tendencies of the char residue at 550 °C and at maximum degradation temperature at various heating rates are shown in Figure 7a,b. The percentage of char residue increased from 3.62% to 6.55% with an increase in the heating rate.

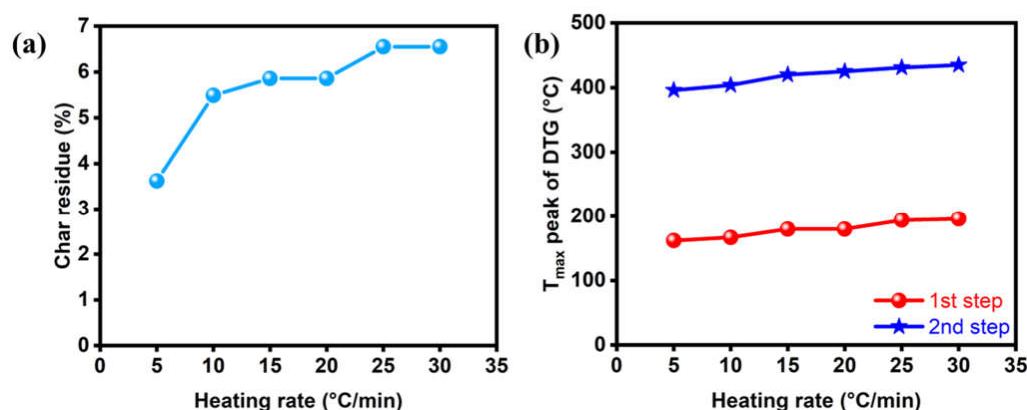


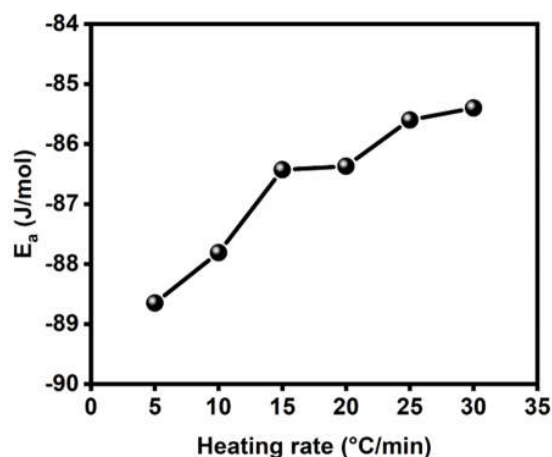
Figure 7. (a) Char residue at 550 °C and (b) T_{max} peak of DTG of PCL-g-MA at a maximum grafting ratio and degradation temperature as a function of heating rate.

The relationships between $\ln(g(\alpha)/T^2)$ and T^{-1} according to Equation (8) using differential function $g(\alpha)$ from Table 4 are shown in Table 5. The kinetic models were chosen from the linear approximation to be with a high determination coefficient (R^2). Table 5 shows model R3 provided the linear trend with a higher determination coefficient (R^2 equals approx. 0.99) than the other models with α from TGA-simulated curves with the spherical symmetry based on the Geometrical Contraction Model (R3) based on the Coats–Redfern method for the reaction of the modification of PCL-g-MA. These models and results indicate the pyrolysis of the PCL-g-MA structure so that the positions of MA grafted on a PCL main chain are more likely to undergo random scissions first due to the weak bonding from C-C structure to produce shorter monomers and generate free radicals of the polymer. After that, the PCL structure starts to degrade by random scissions via cis-elimination reactions and progresses with cyclic rupture via intramolecular transesterification at over 300 °C [74,81]. The pyrolysis results confirmed the same tendency as suggested by the TGA and DTA results in Figure 6.

Table 5. Determination coefficient R^2 calculated from kinetic parameters for different models with α values obtained from TGA-simulated curves by the Coats–Redfern equation.

Mechanism Models	Heating Rate ($^{\circ}\text{C}/\text{min}$)					
	5	10	15	20	25	30
Order of Reaction						
First order (F1)	0.8780	0.7861	0.5476	0.3249	0.1594	0.0849
Second order (F2)	0.8058	0.7271	0.7021	0.6985	0.6826	0.7069
Third order (F3)	0.6923	0.5948	0.5856	0.5562	0.5722	0.5719
Diffusion Models						
One-dimensional diffusion (D1)	0.9581	0.6746	0.3735	0.1831	0.0689	0.0293
Two-dimensional diffusion (D2)	0.8877	0.9329	0.8959	0.9465	0.8998	0.9338
Three-dimensional diffusion, Jandel (D3)	0.9200	0.8251	0.7380	0.7189	0.6116	0.5684
Diffusion control, Ginstling–Brounshtein (D4)	0.8956	0.8368	0.8131	0.8015	0.7905	0.7839
Nucleation Growth Models						
Two-dimensional (A2)	0.8800	0.8953	0.8588	0.9038	0.8400	0.8935
Three-dimensional (A3)	0.8800	0.8953	0.8588	0.9038	0.8400	0.8935
Four-dimensional (A4)	0.8800	0.8953	0.8588	0.9038	0.8400	0.8935
Geometrical Contraction Model						
One dimension (R1)	0.7936	0.8000	0.5663	0.3236	0.1403	0.0639
Two dimensions (R2)	0.9683	0.9282	0.8875	0.8803	0.8277	0.8037
Three dimensions (R3)	0.9949	0.9888	0.9839	0.9822	0.9747	0.9706
Experimental Nucleation Models						
Power law (P2)	0.7936	0.8000	0.5663	0.3236	0.1403	0.06386
Power law (P3)	0.7936	0.8000	0.5663	0.3236	0.1403	0.06386
Power law (P4)	0.7936	0.8000	0.5663	0.3236	0.1403	0.06386

Consequently, model R3 was the most suitable model to explain the thermal decomposition of the synthesized PCL-g-MA, where the E_a of model R3 was calculated and is shown in Figure 8. The E_a is expressed in the exothermal reaction of the modification of PCL-g-MA (detailed information in supplementary material Table S10). E_a is the parameter that is represented to be evaluated from the thermogravimetric analysis because the thermal breakage of the chemical bonds of the polymer provided the solid–gas conversion of the biomass in combustible gas, and E_a may also provide the needed energy information for starting the chemical decomposition. Thus, the exothermal reaction could be related to the breakage of the C–C bonds of the polymers [82].

**Figure 8.** Activation energies calculated based on the contracting volume model (R3) at various heating rates.

4. Conclusions

An optimum condition to synthesise PCL-g-MA with the highest grafting ratio was determined by the measurement of FTIR spectra, which provided peaks at 1790 and 1867 cm^{-1} attributed to maleic anhydride. This result indicates a successful grafting of MA on PCL surfaces. Factors involved with the high grafting ratio were the amount of DBPO and MA, and the reaction period. The optimum condition was 1.120 g and the amount of MA added 3.000 g for a reaction time of 18 h. Additionally, the results of the contact angle also confirmed the relationship between the grafting ratio and the hydrophilic property. The hydrophilic property was increased by the grafting of MA on PCL. The thermal stability of PCL-g-MA decreased with the increasing amount of grafted MA. The PCL-g-MA synthesised at an optimum condition was analysed using TGA at various heating rates from 5–30 $^{\circ}\text{C}/\text{min}$ at an interval of 5 $^{\circ}\text{C}/\text{min}$, and then all the TGA data were explained with the Coats–Redfern equation to find the best fitting kinetic model. The results of the TGA analysis were plotted as $\ln(g(\alpha)/T^2)$ as a function of $1/T$ for different kinetic models using different values of $g(\alpha)$. The highest determination coefficient R^2 was obtained when applying a linear regression based on the spherical symmetry diffusion mechanism (R3), suggesting this model is suitable for explaining the synthesis of PCL-g-MA. After that, E_a was calculated and expressed in the exothermal reaction of the modification of PCL-g-MA that explained the relation of the breaking of the carbon–carbon bonds of the polymers.

Supplementary Materials: The following supporting information can be downloaded at: <https://www.mdpi.com/article/10.3390/polym14194100/s1>, Figure S1: Thermograms of PCL-g-MA; Figure S2: Derivative thermogravimetric analysis (DTG) of PCL-g-MA; Figure S3: Differential scanning calorimetry (DSC) thermograms; Figure S4: X-ray Diffraction (XRD) of (a) PCL and MA, PCL-g-MA; Figure S5: Nuclear Magnetic Resonance (NMR) of (a) PCL, (b) MA, and (c) PCL-g-MA [83,84]; Figure S6: High resolution XPS spectra for C1s and O1s of various reaction time; Figure S7: High resolution XPS spectra for C1s and O1s of various MA added; Figure S8: High resolution XPS spectra for C1s and O1s of various DBPO added; Table S1–S4: Summary of DSC measurement results; Table S5–S8: Summary of the high-resolution results; Table S9: Summary of the T_i , T_{max} , T_f , DTG at main T_{max} peak and residue at 550 $^{\circ}\text{C}$ at the different heating rates; Table S10: Activation energy calculated based on the contracting volume model (R3) at various heating rates.

Author Contributions: Conceptualization, K.T. and D.H.; formal analysis, K.T., X.S. and D.H.; writing—original draft preparation, K.T.; writing—review and editing, D.H. and T.E.; supervision, D.H., M.K., M.A.N. and T.E.; funding acquisition, T.E. All authors have read and agreed to the published version of the manuscript.

Funding: This research was funded by a joint-research fund of academic–industrial alliance with Wacom Co. Ltd. (CDI03138) and the funding from the operating budget of University of Tsukuba.

Institutional Review Board Statement: Not applicable.

Data Availability Statement: The data presented in this study are available on request from the corresponding authors.

Acknowledgments: T. Kotchaporn acknowledges the Ministry of Education, Culture, Sports, Science and Technology (MEXT) of Japan for providing the scholarship under the Trans-world Professional Human Resources Development Program on Food Security & Natural Resources Management (TPHRD) for Doctoral Course.

Conflicts of Interest: Authors declared no conflict of interest.

References

1. Geyer, R.; Jambeck, J.R.; Law, K.L. Production, use, and fate of all plastics ever made. *Sci. Adv.* **2017**, *3*, e1700782. [[CrossRef](#)] [[PubMed](#)]
2. Haque, M.; Errico, M.; Gentile, G.; Avella, M.; Pracella, M. Functionalization and compatibilization of poly(ϵ -caprolactone) composites with cellulose microfibrils. *Macromol. Mater. Eng.* **2012**, *297*, 985–993. [[CrossRef](#)]
3. Chen, Y.; Awasthi, A.K.; Wei, F.; Tan, Q.; Li, J. Single-use plastics: Production, usage, disposal, and adverse impacts. *Sci. Total Environ.* **2021**, *752*, 141772. [[CrossRef](#)] [[PubMed](#)]

4. Andrady, A.L.; Neal, M.A. Applications and societal benefits of plastics. *Philos. Trans. R. Soc. Lond. B Biol. Sci.* **2009**, *364*, 1977–1984. [[CrossRef](#)] [[PubMed](#)]
5. MacDiarmid, A.G. “Synthetic Metals”: A Novel Role for Organic Polymers (Nobel Lecture). *Angew. Chem. Int. Ed.* **2001**, *40*, 2581–2590. [[CrossRef](#)]
6. Sengwa, R.J.; Choudhary, S.; Dhatarwal, P. Investigation of alumina nanofiller impact on the structural and dielectric properties of PEO/PMMA blend matrix-based polymer nanocomposites. *Adv. Compos. Mater.* **2019**, *2*, 162–175. [[CrossRef](#)]
7. Diaz Silvarrey, L.S.; Phan, A.N. Kinetic study of municipal plastic waste. *Int. J. Hydrogen Energy* **2016**, *41*, 16352–16364. [[CrossRef](#)]
8. Barnes, S.J. Out of sight, out of mind: Plastic waste exports, psychological distance and consumer plastic purchasing. *Glob. Environ. Change* **2019**, *58*, 101943. [[CrossRef](#)]
9. Brebu, M. Environmental Degradation of Plastic Composites with Natural Fillers—A Review. *Polymers* **2020**, *12*, 166. [[CrossRef](#)]
10. Cox, K.D.; Covernton, G.A.; Davies, H.L.; Dower, J.F.; Juanes, F.; Dudas, S.E. Human Consumption of Microplastics. *Environ. Sci. Technol.* **2019**, *53*, 7068–7074. [[CrossRef](#)]
11. Filho, W.L.; Havea, P.H.; Balogun, A.-L.; Boenecke, J.; Maharaj, A.A.; Ha’apio, M.; Hemstock, S.L. Plastic debris on Pacific Islands: Ecological and health implications. *Sci. Total Environ.* **2019**, *670*, 181–187. [[CrossRef](#)]
12. Steensgaard, I.M.; Syberg, K.; Rist, S.; Hartmann, N.B.; Boldrin, A.; Hansen, S.F. From macro- to microplastics—Analysis of EU regulation along the life cycle of plastic bags. *Environ. Pollut.* **2017**, *224*, 289–299. [[CrossRef](#)]
13. Jambeck, J.R.; Geyer, R.; Wilcox, C.; Siegler, T.R.; Perryman, M.; Andrady, A.; Narayan, R.; Law, K.L. Plastic waste inputs from land into the ocean. *Science* **2015**, *347*, 768–771. [[CrossRef](#)]
14. Comanita, E.-D.; Hlihor, R.M.; Ghinea, C.; Gavrilesco, M. Occurrence of Plastic Waste in the Environment: Ecological and Health Risks. *Environ. Eng. Manag. J.* **2016**, *15*, 675–685. [[CrossRef](#)]
15. Ghodrat, M.; Abascal Alonso, J.; Hagare, D.; Yang, R.; Samali, B. Economic feasibility of energy recovery from waste plastic using pyrolysis technology: An Australian perspective. *Int. J. Environ. Sci. Technol.* **2019**, *16*, 3721–3734. [[CrossRef](#)]
16. Hatti-Kaul, R.; Nilsson, L.J.; Zhang, B.; Rehnberg, N.; Lundmark, S. Designing Biobased Recyclable Polymers for Plastics. *Trends Biotechnol.* **2020**, *38*, 50–67. [[CrossRef](#)]
17. Ennis, R. Plastigone, a new time controlled photodegradable plastic mulch film. *Proc. Natl. Agr. Plast. Congr.* **1987**, *20*, 83–90.
18. Moharir, R.V.; Kumar, S. Challenges associated with plastic waste disposal and allied microbial routes for its effective degradation: A comprehensive review. *J. Clean. Prod.* **2019**, *208*, 65–76. [[CrossRef](#)]
19. Goldberg, D. A review of the biodegradability and utility of poly (caprolactone). *J. Environ. Polym. Degrad.* **1995**, *3*, 61–67. [[CrossRef](#)]
20. Sudesh, K.; Iwata, T. Sustainability of Biobased and Biodegradable Plastics. *CLEAN Soil Air Water* **2008**, *36*, 433–442. [[CrossRef](#)]
21. Ganesh Kumar, A.; Anjana, K.; Hinduja, M.; Sujitha, K.; Dharani, G. Review on plastic wastes in marine environment—Biodegradation and biotechnological solutions. *Mar. Pollut. Bull.* **2020**, *150*, 110733.
22. Ohnishi, S.; Fujii, M.; Fujita, T.; Matsumoto, T.; Dong, L.; Akiyama, H.; Dong, H. Comparative analysis of recycling industry development in Japan following the Eco-Town program for eco-industrial development. *J. Clean. Prod.* **2016**, *114*, 95–102. [[CrossRef](#)]
23. Zhang, L.; Xu, Z. Towards minimization of secondary wastes: Element recycling to achieve future complete resource recycling of electronic wastes. *Waste Manag.* **2019**, *96*, 175–180. [[CrossRef](#)]
24. Rai, P.; Mehrotra, S.; Priya, S.; Gnansounou, E.; Sharma, S.K. Recent advances in the sustainable design and applications of biodegradable polymers. *Bioresour. Technol.* **2021**, *325*, 124739. [[CrossRef](#)]
25. Perrin, D.E.; English, J.P. *Handbook of Biodegradable Polymers*; Hardwood Academic Publishers Imprint: Amsterdam, The Netherlands, 1998.
26. Dash, T.K.; Konkimalla, V.B. Polymeric Modification and Its Implication in Drug Delivery: Poly- ϵ -caprolactone (PCL) as a Model Polymer. *Mol. Pharm.* **2012**, *9*, 2365–2379. [[CrossRef](#)]
27. Grossen, P.; Witzigmann, D.; Sieber, S.; Huwyler, J. PEG-PCL-based nanomedicines: A biodegradable drug delivery system and its application. *J. Control. Release* **2017**, *260*, 46–60. [[CrossRef](#)]
28. Rai, B.; Teoh, S.H.; Hutmacher, D.W.; Cao, T.; Ho, K.H. Novel PCL-based honeycomb scaffolds as drug delivery systems for rhBMP-2. *Biomaterials* **2005**, *26*, 3739–3748. [[CrossRef](#)]
29. Holländer, J.; Genina, N.; Jukarainen, H.; Khajeheian, M.; Rosling, A.; Mäkilä, E.; Sandler, N. Three-Dimensional Printed PCL-Based Implantable Prototypes of Medical Devices for Controlled Drug Delivery. *J. Pharm. Sci.* **2016**, *105*, 2665–2676. [[CrossRef](#)]
30. Zhang, J.; Zhao, S.; Zhu, M.; Zhu, Y.; Zhang, Y.; Liu, Z.; Zhang, C. 3D-printed magnetic Fe₃O₄/MBG/PCL composite scaffolds with multifunctionality of bone regeneration, local anticancer drug delivery and hyperthermia. *J. Mater. Chem. B* **2014**, *2*, 7583–7595. [[CrossRef](#)]
31. Tous, L.; Ruseckaitė, R.A.; Ciannamea, E.M. Sustainable hot-melt adhesives based on soybean protein isolate and polycaprolactone. *Ind. Crops Prod.* **2019**, *135*, 153–158. [[CrossRef](#)]
32. Laine, C.; Willberg-Keyriläinen, P.; Ropponen, J.; Liitiä, T. Lignin and lignin derivatives as components in biobased hot melt adhesives. *J. Appl. Polym. Sci.* **2019**, *136*, 47983. [[CrossRef](#)]
33. Cheng, H.N.; Ford, C.V.; He, Z. Evaluation of polyblends of cottonseed protein and polycaprolactone plasticized by cottonseed oil. *Int. J. Polym. Anal. Charact.* **2019**, *24*, 389–398. [[CrossRef](#)]

34. Sailema-Palate, G.P.; Vidaurre, A.; Campillo-Fernández, A.J.; Castilla-Cortázar, I. A comparative study on Poly (ϵ -caprolactone) film degradation at extreme pH values. *Polym. Degrad. Stab.* **2016**, *130*, 118–125. [[CrossRef](#)]
35. Bartnikowski, M.; Dargaville, T.R.; Ivanovski, S.; Hutmacher, D.W. Degradation mechanisms of polycaprolactone in the context of chemistry, geometry and environment. *Prog. Polym. Sci.* **2019**, *96*, 1–20. [[CrossRef](#)]
36. Von Burkersroda, F.; Schedl, L.; Göpferich, A. Why degradable polymers undergo surface erosion or bulk erosion. *Biomaterials* **2002**, *23*, 4221–4231. [[CrossRef](#)]
37. Jawaid, M.; Khalil, H.A. Cellulosic/synthetic fibre reinforced polymer hybrid composites: A review. *Carbohydr. Polym.* **2011**, *86*, 1–18. [[CrossRef](#)]
38. Chen, S.; Zhang, Z.-L.; Song, F.; Wang, X.-L.; Wang, Y.-Z. Rapid Synthesis of Polymer-Grafted Cellulose Nanofiber Nanocomposite via Surface-Initiated Cu(0)-Mediated Reversible Deactivation Radical Polymerization. *Macromolecules* **2021**, *54*, 7409–7420. [[CrossRef](#)]
39. Pracella, M.; Haque, M.M.-U.; Alvarez, V. Functionalization, Compatibilization and Properties of Polyolefin Composites with Natural Fibers. *Polymers* **2010**, *2*, 554–574. [[CrossRef](#)]
40. John, J.; Tang, J.; Yang, Z.; Bhattacharya, M.K. Synthesis and characterization of anhydride-functional polycaprolactone. *J. Polym. Sci. Part A* **1997**, *35*, 1139–1148. [[CrossRef](#)]
41. Mani, R.; Bhattacharya, M.; Tang, J. Functionalization of polyesters with maleic anhydride by reactive extrusion. *J. Polym. Sci. Part A Polym. Chem.* **1999**, *37*, 1693–1702. [[CrossRef](#)]
42. Gardella, L.; Calabrese, M.; Monticelli, O. PLA maleation: An easy and effective method to modify the properties of PLA/PCL immiscible blends. *Colloid Polym. Sci.* **2014**, *292*, 2391–2398. [[CrossRef](#)]
43. Qiu, W.; Hirotsu, T. A New Method to Prepare Maleic Anhydride Grafted Poly(propylene). *Macromol. Chem. Phys.* **2005**, *206*, 2470–2482. [[CrossRef](#)]
44. Beyer, G.; Hopmann, C. *Reactive Extrusion: Principles and Applications*; Wiley-VCH Verlag GmbH & Co.KGaA, Boschstr: Weinheim, Germany, 2018.
45. Ahmad Thirmizir, M.; Mohd Ishak, Z.; Mat Taib, R.; Rahim, S.; Mohamad Jani, S. Natural weathering of kenaf bast fibre-filled poly (butylene succinate) composites: Effect of fibre loading and compatibiliser addition. *J. Polym. Environ.* **2011**, *19*, 263–273. [[CrossRef](#)]
46. Khankrua, R.; Pivsa-Art, S.; Hiroyuki, H.; Suttiruengwong, S. Thermal and Mechanical Properties of Biodegradable Polyester/Silica Nanocomposites. *Energy Procedia* **2013**, *34*, 705–713. [[CrossRef](#)]
47. Singh, S.K.; Sawarkar, A.N. Thermal decomposition aspects and kinetics of pyrolysis of garlic stalk. *Energy Sources A Recovery Util. Environ. Eff.* **2020**, 1–11. [[CrossRef](#)]
48. Shih, Y.-F.; Chieh, Y.-C. Thermal Degradation Behavior and Kinetic Analysis of Biodegradable Polymers Using Various Comparative Models, 1. *Macromol. Theory Simul.* **2007**, *16*, 101–110. [[CrossRef](#)]
49. Cai, J.; Bi, L. Precision of the Coats and Redfern Method for the Determination of the Activation Energy without Neglecting the Low-Temperature End of the Temperature Integral. *Energy Fuels* **2008**, *22*, 2172–2174. [[CrossRef](#)]
50. Ramukutty, S.; Ramachandran, E. Reaction Rate Models for the Thermal Decomposition of Ibuprofen Crystals. *J. Cryst. Process Technol.* **2014**, *4*, 71–78. [[CrossRef](#)]
51. Coats, A.W.; Redfern, J. Kinetic parameters from thermogravimetric data. *Nature* **1964**, *201*, 68–69. [[CrossRef](#)]
52. Wu, C.-S.; Liao, H.-T. Polycaprolactone-Based Green Renewable Ecocomposites Made from Rice Straw Fiber: Characterization and Assessment of Mechanical and Thermal Properties. *Ind. Eng. Chem. Res.* **2012**, *51*, 3329–3337. [[CrossRef](#)]
53. Nakason, C.; Kaesaman, A.; Supasanthitkul, P. The grafting of maleic anhydride onto natural rubber. *Polym. Test.* **2004**, *23*, 35–41. [[CrossRef](#)]
54. Ma, Q.; Shi, K.; Su, T.; Wang, Z. Biodegradation of Polycaprolactone (PCL) with Different Molecular Weights by Candida antarctica Lipase. *J. Polym. Environ.* **2020**, *28*, 2947–2955. [[CrossRef](#)]
55. Wang, Q.; Ji, C.; Sun, J.; Yao, Q.; Liu, J.; Saeed, R.M.Y.; Zhu, Q. Kinetic thermal behavior of nanocellulose filled polylactic acid filament for fused filament fabrication 3D printing. *J. Appl. Polym. Sci.* **2020**, *137*, 48374. [[CrossRef](#)]
56. Salla, J.M.; Morancho, J.M.; Cadenato, A.; Ramis, X. Non-isothermal degradation of a thermoset powder coating in inert and oxidant atmospheres. *J. Therm. Anal. Calorim.* **2003**, *72*, 719–728. [[CrossRef](#)]
57. Ramis, X.; Cadenato, A.; Morancho, J.M.; Salla, J.M. Curing of a thermosetting powder coating by means of DMTA, TMA and DSC. *Polymer* **2003**, *44*, 2067–2079. [[CrossRef](#)]
58. Ramis, X.; Salla, J.; Cadenato, A.; Morancho, J.M. Simulation of isothermal cure of a powder coating—Non-isothermal DSC experiments. *J. Therm. Anal. Calorim.* **2003**, *72*, 707–718. [[CrossRef](#)]
59. Ramis, X.; Cadenato, A.; Salla, J.; Morancho, J.M.; Vallés, A.; Contat, L.; Amparo, R. Thermal Degradation of Polypropylene/starch-based materials with enhanced biodegradability. *Polym. Degrad. Stab.* **2004**, *86*, 483–491. [[CrossRef](#)]
60. Barra, G.; Crespo, J.; Bertolino, J.; Soldi, V.; Nunes, P. Maleic Anhydride Grafting on EPDM: Qualitative and Quantitative Determination. *J. Braz. Chem. Soc.* **1999**, *10*, 31–34. [[CrossRef](#)]
61. Vilay, V.; Mariatti, M.; Ahmad, Z.; Pasomsouk, K.; Todo, M. Improvement of microstructures and properties of biodegradable PLLA and PCL blends compatibilized with a triblock copolymer. *Mater. Sci. Eng. A* **2010**, *527*, 6930–6937. [[CrossRef](#)]

62. Azizi, M.; Azimzadeh, M.; Afzali, M.; Alafzadeh, M.; Mirhosseini, S. Characterization and optimization of using calendula officinalis extract in fabrication of polycaprolactone-gelatin electrospun nanofibers for wound dressing applications. *J. Adv. Mater. Process.* **2018**, *6*, 34–46.
63. Qiu, W.; Endo, T.; Hirotsu, T. A novel technique for preparing of maleic anhydride grafted polyolefins. *Eur. Polym. J.* **2005**, *41*, 1979–1984. [[CrossRef](#)]
64. Yang, L.; Zhang, F.; Endo, T.; Hirotsu, T. Microstructure of Maleic Anhydride Grafted Polyethylene by High-Resolution Solution-State NMR and FTIR Spectroscopy. *Macromolecules* **2003**, *36*, 4709–4718. [[CrossRef](#)]
65. Permyakova, E.S.; Kiryukhantsev-Korneev, P.V.; Guduz, K.Y.; Konopatsky, A.S.; Polčák, J.; Zhitnyak, I.Y.; Gloushankova, N.A.; Shtansky, D.V.; Manakhov, A.M. Comparison of Different Approaches to Surface Functionalization of Biodegradable Polycaprolactone Scaffolds. *Nanomaterials* **2019**, *9*, 1769. [[CrossRef](#)]
66. Kim, J.; Mousa, H.M.; Park, C.H.; Kim, C.S. Enhanced corrosion resistance and biocompatibility of AZ31 Mg alloy using PCL/ZnO NPs via electrospinning. *Appl. Surf. Sci.* **2017**, *396*, 249–258. [[CrossRef](#)]
67. Wang, H.; Li, Z.; Hong, K.; Chen, M.; Qiao, Z.; Yuan, Z.; Wang, Z. Property improvement of multi-walled carbon nanotubes/polypropylene composites with high filler loading via interfacial modification. *RSC Adv.* **2019**, *9*, 29087–29096. [[CrossRef](#)]
68. Chen, C.; Peng, S.; Fei, B.; Zhuang, Y.; Dong, L.; Feng, Z.; Chen, S.; Xia, H. Synthesis and characterization of maleated poly(3-hydroxybutyrate). *J. Appl. Polym. Sci.* **2003**, *88*, 659–668. [[CrossRef](#)]
69. Takamura, M.; Nakamura, T.; Takahashi, T.; Koyama, K. Effect of type of peroxide on cross-linking of poly(l-lactide). *Polym. Degrad. Stab.* **2008**, *93*, 1909–1916. [[CrossRef](#)]
70. Bhattacharya, A.; Misra, B.N. Grafting: A versatile means to modify polymers: Techniques, factors and applications. *Prog. Polym. Sci.* **2004**, *29*, 767–814. [[CrossRef](#)]
71. Bátor, V.; Lundin, M.; Åkesson, D.; Lennartsson, P.R.; Taherzadeh, M.J.; Zamani, A. The Effect of Glycerol, Sugar, and Maleic Anhydride on Pectin-Cellulose Thin Films Prepared from Orange Waste. *Polymers* **2019**, *11*, 392. [[CrossRef](#)]
72. Leluk, K.; Kozłowski, M. Thermal and mechanical properties of flax-reinforced polycaprolactone composites. *Fibers Polym.* **2014**, *15*, 108–116. [[CrossRef](#)]
73. Morais, D.; Siqueira, D.; Bruno Barreto Luna, C.; Araujo, E.; Bezerra, E.; Wellen, R. Grafting Maleic Anhydride onto Polycaprolactone: Influence of processing. *Mater. Res. Express* **2019**, *6*, 055315. [[CrossRef](#)]
74. Papageorgiou, D.G.; Roumeli, E.; Terzopoulou, Z.; Tsanaktis, V.; Chrissafis, K.; Bikiaris, D. Polycaprolactone/multi-wall carbon nanotube nanocomposites prepared by in situ ring opening polymerization: Decomposition profiling using thermogravimetric analysis and analytical pyrolysis–gas chromatography/mass spectrometry. *J. Anal. Appl. Pyrolysis* **2015**, *115*, 125–131. [[CrossRef](#)]
75. Ortega-Toro, R.; Santagata, G.; Gomez d’Ayala, G.; Cerruti, P.; Talens Oliag, P.; Chiralt Boix, M.A.; Malinconico, M. Enhancement of interfacial adhesion between starch and grafted poly(ϵ -caprolactone). *Carbohydr. Polym.* **2016**, *147*, 16–27. [[CrossRef](#)]
76. Lopera-Valle, A.; Elias, A. Amine Responsive Poly (lactic acid) (PLA) and Succinic Anhydride (SAh) Graft-Polymer: Synthesis and Characterization. *Polymers* **2019**, *11*, 1466. [[CrossRef](#)]
77. Simão, J.A.; Bellani, C.F.; Branciforti, M.C. Thermal properties and crystallinity of PCL/PBSA/cellulose nanocrystals grafted with PCL chains. *J. Appl. Polym. Sci.* **2017**, *134*, 44493. [[CrossRef](#)]
78. Wang, G.; Yang, S.; Wei, Z.; Dong, X.; Wang, H.; Qi, M. Facile preparation of poly(ϵ -caprolactone)/Fe₃O₄@graphene oxide superparamagnetic nanocomposites. *Polym. Bull.* **2013**, *70*, 2359–2371. [[CrossRef](#)]
79. Huang, Y.; Fan, C.; Han, X.; Jiang, X. A TGA-MS investigation of the effect of heating rate and mineral matrix on the pyrolysis of kerogen in oil shale. *Oil Shale* **2016**, *33*, 125. [[CrossRef](#)]
80. Wongthong, P.; Nakason, C.; Pan, Q.; Rempel, G.L.; Kiatkamjornwong, S. Modification of deproteinized natural rubber via grafting polymerization with maleic anhydride. *Eur. Polym. J.* **2013**, *49*, 4035–4046. [[CrossRef](#)]
81. Zhang, Y.; Fu, Z.; Wang, W.; Ji, G.; Zhao, M.; Li, A. Kinetics, Product Evolution, and Mechanism for the Pyrolysis of Typical Plastic Waste. *ACS Sustain. Chem. Eng.* **2021**, *10*, 91–103. [[CrossRef](#)]
82. Da Silva, J.; Alves, J.L.; Galdino, W.; Moreira, R.; José, H.; Sena, R.; Andersen, S. Combustion of pistachio shell: Physicochemical characterization and evaluation of kinetic parameters. *Environ. Sci. Pollut. Res.* **2018**, *25*, 21420–21429. [[CrossRef](#)]
83. Fulmer, G.R.; Miller, A.J.M.; Sherden, N.H.; Gottlieb, H.E.; Nudelman, A.; Stoltz, B.M.; Bercaw, J.E.; Goldberg, K.I. NMR Chemical Shifts of Trace Impurities: Common Laboratory Solvents, Organics, and Gases in Deuterated Solvents Relevant to the Organometallic Chemist. *Organometallics* **2010**, *29*, 2176–2179. [[CrossRef](#)]
84. Khankrua, R.; Pivsa-Art, S.; Hiroyuki, H.; Suttiruengwong, S. Grafting of poly (lactic acid) with maleic anhydride using supercritical carbon dioxide. *IOP Conf. Ser.: Mater. Sci. Eng.* **2015**, *87*, 12066. [[CrossRef](#)]